COBEM 2023 27TH INTERNATIONAL CONGRESS OF MECHANICAL ENGENEERING

ABCM Brazilian Society of Mechanical Sciences and Engineering
27th ABCM International Congress of Mechanical Engineering
December 04-08, 2023, Florianópolis-SC, Brazil

COB-2023-1491
FINITE INTEGRAL TRANSFORM ANALYSIS WITH HOMOGENIZED TIME-DEPENDENT BOUNDARY CONDITIONS OF 2-D CYLINDRICAL MULTI-LAYER COMPOSITES SOLUTION FOR TRANSIENT HEAT CONDUCTION APPLIED TO PLUG AND ABANDONMENT OF OIL WELLS

Gabriel Saavedra de Andrade
Marcelo José Santos de Lemos
Instituto Tecnológico de Aeronáutica – São José dos Campos
gasaavedra.eme@gmail.com ; delemos@ita.br

Abstract. *An analytical method for transient heat conduction problem is applied to Plug and Abandonment (P&A) operations of oil wells. An oil well is approximated to a concentric composite cylinder geometry, characterizing the governing equations to be cast in radial-azimuthal polar coordinates. Plug and Abandonment operations are performed when the oil well provides no attractive return of capital, being a practice where the expenditure must be mitigated. This scenario opened opportunities to develop a new technology devoted to plug oil wells called Thermal Plug and Abandonment (TP&A), which substitutes the use of cement in usual practices with the use of an energetic mixture able to melt the oil well structures, sealing the whole cross-section with the solidification of the melted components. This proposal is able to diminish the number of required maneuvers in view of the usual P&A practices, reducing the daily rig rental cost and saving a great of capital expenditure by doing so. The application of the Finite Integral Transform (FIT) technique is a mathematical framework able to solve efficiently the transient heat conduction when prescribed time-dependent boundary conditions. However, the FIT approach is able to solve only boundary conditions of Neumann type. Performing the homogenization of the prescribed boundary conditions allows the application of FIT to any type of boundary condition, which generalizes the analytical approach applied to the TP&A procedure, where the problem setup requires the prescription of boundary condition of Dirichlet type. Plus, as the energic mixture is a time-dependent volumetric heat source set in the inner most layer of the composite domain, the analytical method available in this work has relevant advantages in comparison with other well-known analytical approaches. Lastly, the obtained results throughout the composite cylindrical domain achieves relevant content, subsidizing the new proposed technology by meeting regulatory normative requirements established to P&A operations.*

Keywords: *Analytical Transient Heat Conduction, Plug & Abandonment, Finite Integral Transform, Composite Cylinder Domain, Homogenization*

1. INTRODUCTION

Composite laminates offer advantages in engineering applications, depending on the desired thermal effects. These effects can include enhancement, dissipation, or maintenance of heat diffusion phenomena. Achieving these desired heat conduction behaviors often involves combining materials with distinct thermophysical properties to create multi-layered domains. In the case of composite cylinders, which are of particular interest in the oil and gas industry, such multi-layered structures have applications in various areas, including ground heat exchangers (Gu & O'Neal, 1995), circular Micro-Hotplate (MHP) (Torabi & Zhang, 2016), pipeline with Phase Change Material (PCM) particles (Wang, Duan, An, & Su, 2021) and tunnel lining heating systems (Zhang, Xia, Sun, Zou, & Xiao, 2013).

A classic oil well assembly typically consists of five concentric hollow cylinders. The innermost layer, known as the production tube, is made of stainless steel (SS AISI 420) and transports oil from the reservoir to the platform. The layer adjacent to it is the "A-annulus," which is often filled with mud or water. The next layer provides structural support and is typically made of API X80 steel casing. The outer layers consist of class G Portland cement and the geological formation, often composed of a sedimentary rock called "cap rock," typically dolomite.

When it comes to decommissioning an oil well, one critical operation is the Plug and Abandonment (P&A) procedure, which can account for a significant portion of the overall decommissioning cost (Ouyang & Allen, 2017). Usual P&A procedures require the installation of permanent cement barriers within the A-annulus region (Abshire, et al., 2012). This procedure necessitates removing the production tube, a time-consuming and costly endeavor. To reduce costs and make the process more efficient many technologies devoted to enhancing P&A operations are being investigated (Vrålstad, Saasen, Fjær, Øia, & Ytre, 2019). Alternative methods, such as the "through tubing" approach, have been explored (Moeinikia, Fjelde, Sørbø, Saasen, & Vrålstad, 2015). In this approach, plugging the well doesn't require removing the

production tube. Instead, a heat emitter device, powered by a thermite chemical reaction, is used to melt the production tube, creating a plug to seal the well. This approach will be here termed as Thermal Plug and Abandonment (TP&A) procedure, as investigated in previous work (de Andrade, de Lemos, & Colombo, 2021).

However, the "through tubing" method raises concerns about the control lines attached to the production tube, as cement placed in the annulus region may result in micro-annuli formation, potentially causing leakage (Aas, et al., 2016). To address this issue, an intermediate milestone with two stages is proposed. The first stage focuses on melting the production tube entirely during the thermite reaction, creating a gap section below the operational site. The second stage involves removing the control lines and then pumping cement downhole to seal the well properly.

Introduced the TP&A concepts, the transient thermal behavior resultant from the time-dependent volumetric heat source arising from the thermite reaction can be investigated by either analytical or numerical approaches. Also, in view of both stages of the intermediate milestone proposed, the composite cylinder domain will be here cast in two-dimensional polar coordinates. The main objective herein is to apply the analytical methodology to provide an equating that can solve the heat transfer physics behind the unprecedent TP&A proposition. Plus, the mathematical modeling of an engineering application elucidates one about the occurring phenomena by offering the possibility of being employed as an additional verification tool for numerical approaches under development.

To investigate the transient thermal behavior resulting from the time-dependent volumetric heat source of the thermite reaction, analytical and numerical methods are employed. This research focuses on applying the Finite Integral Transform (FIT) technique to solve the heat transfer physics behind the TP&A procedure. The FIT technique deals with spatial terms, similar to the Laplace transform's treatment of temporal terms. However, for efficient application, the 2-D transient heat conduction equation in polar coordinates must be transformed into sets of 1-D equations using the Orthogonal Eigenfunction Expansion (OEE). This reduction allows for the application of integral transforms to the remaining spatial term, resulting in a system of 1-D Ordinary Differential Equations (ODEs) dependent only on the temporal term. The solution to these ODEs is straightforward, and the main 2-D PDE is solved through an inversion technique. This framework accommodates spatial-temporal volumetric heat sources and boundary conditions. However, when dealing with non-homogenized boundary conditions, FIT cannot solve problems with Dirichlet-type boundary conditions (Biswas, Singh, & Bindra, 2019). Therefore, homogenizing the boundary conditions becomes necessary.

Homogenizing the boundary conditions involves splitting the problem into a homogeneous transient problem and a nonhomogeneous pseudo-steady-state problem. After solving these separately and combining the solutions, FIT with homogenized boundary conditions can be applied to 2-D transient heat conduction problems in polar coordinates, accommodating various time-dependent boundary conditions.

This work applies the FIT technique with homogenized boundary conditions to investigate the TP&A procedure. It allows for the consideration of conditions required in the TP&A problem, including the time-dependent asymmetrical behavior of the volumetric heat source from the thermite reaction (de Andrade, Nascimento, & de Lemos, 2023). The results contribute to fulfilling the first and second intermediate milestone requirements by tracing radial and azimuthal transient thermal fields, respectively. Additionally, contour plots reveal insights into regions of high-temperature gradients, particularly in the azimuthal portion of the production tube thickness. Filling the Annular-A region with water is shown to effectively protect the cement layer from extreme temperature levels, mitigating potential adverse effects caused by substantial temperature variations.

2. MATHEMATICAL MODELING

The unsteady heat conduction governing equation in 2-D polar coordinates with constant thermophysical properties, perfect thermal contact between interfaces, and accounting the source term is written as

$$\frac{1}{\alpha_i}\frac{\partial T_i}{\partial t}(r,\theta,t)=\frac{1}{r}\frac{\partial}{\partial r}\left(r\frac{\partial T_i}{\partial r}(r,\theta,t)\right)+\frac{1}{r^2}\frac{\partial^2 T_i}{\partial \theta^2}(r,\theta,t)+\frac{g_i(r,\theta,t)}{k_i} \tag{1}$$

where r and θ are the radial and angular coordinates that defines the spatial characteristic of the domain in analysis and t is the time coordinate. The thermophysical properties are defined by k_i and α_i, namely the ith layer associated thermal conductivity and thermal diffusivity, respectively. The spatial-temporal dependent heat source can be prescribed at any layer and is here represented by the $g_i(r,\theta,t)$ term. Lastly, the resultant temperature profile throughout the entire multilayered domain, as depicted in Figure 1, is denominated by $T_i(r,\theta,t)$.

Considering the general case of a composite hollow cylinder domain $(r_0>0)$, the boundary conditions at the inner and outer extremities and the initial condition throughout the domain may be cast as, respectively

$$A_{in}\frac{\partial T_1}{\partial r}(r_0,\theta,t)+B_{in}T_1(r_0,\theta,t)=C_{in}(\theta,t) \tag{2}$$

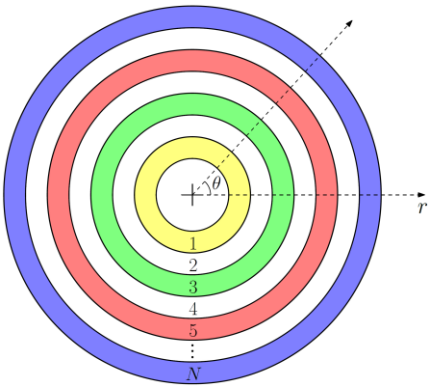

Figure 1 – *N*-layer composite hollow cylinder domain.

$$A_{out}\frac{\partial T_n}{\partial r}(r_n,\theta,t)+B_{out}T_n(r_n,\theta,t)=C_{out}(\theta,t) \tag{3}$$

$$T_i(r,\theta,t=0)=f_i(r,\theta) \tag{4}$$

where A_{in}, B_{in}, C_{in}, A_{out}, B_{out} and C_{out} are the coefficients of the inner and outer boundary conditions that defines the type of boundary value problem being prescribed (Dirichlet, Neumann or Robin). The function $f_i(r,\theta)$ is the initial condition term. The present analysis allows the employment of any kind of boundary conditions, overcoming the limitation of the FIT methodology to be applied only for boundary conditions of boundary.

In the angular direction, a periodic boundary condition is prescribed as follows

$$T_i(r,\theta=0,t)=T_i(r,\theta=2\pi,t) \tag{5}$$

$$\frac{\partial T_i}{\partial\theta}(r,\theta=0,t)=\frac{\partial T_i}{\partial\theta}(r,\theta=2\pi,t) \tag{6}$$

which grantees the continuity of both the temperature and heat flux profiles. The interfacial conditions are cast as

$$T_i(r_{i-1},\theta,t)=T_{i-1}(r_{i-1},\theta,t) \tag{7}$$

$$k_i\frac{\partial T_i}{\partial r}(r_{i-1},\theta,t)=k_{i-1}\frac{\partial T_{i-1}}{\partial r}(r_{i-1},\theta,t) \tag{8}$$

To continue the development of the present methodology, one of the dimensions of the 2-D PDE in Eq. (1) must be reduced and modified, which detailed procedure is discussed along the next sections.

2.1 2-D reduction to a set of 1-D heat conduction problems

Before proceeding with the FIT framework, the theta direction will be reduced here, remaining only the radial direction available to apply the integral transform over. To reduce the azimuthal coordinate, one should make use of the generalized Fourier series expansion devoted to the transient temperature field term, yielding

$$T_i(r,\theta,t)=\sum_{m=0}^{\infty}T_{imc}^{\theta}(r,t)\cos(m\theta)+\sum_{m=1}^{\infty}T_{ims}^{\theta}(r,t)\sin(m\theta) \tag{9}$$

which performing this series expansion degenerates the azimuthal angle from $T_i(r,\theta,t)$ to $T_{im}^{\theta}(r,t)$. The subscripts c and s in Eq. (9) are related to the cosine and sine oscillatory functions, respectively. The same series expansion is applied to each theta dependent function, being represented as follows.

$$g_i(r,\theta,t)=\sum_{m=0}^{\infty}g_{imc}^{\theta}(r,t)\cos(m\theta)+\sum_{m=1}^{\infty}g_{ims}^{\theta}(r,t)\sin(m\theta) \tag{10}$$

$$C_{in}(\theta,t)=\sum_{m=0}^{\infty}C_{in,mc}^{\theta}(t)\cos(m\theta)+\sum_{m=1}^{\infty}C_{in,ms}^{\theta}(t)\sin(m\theta) \tag{11}$$

$$C_{out}(\theta,t)=\sum_{m=0}^{\infty}C_{out,mc}^{\theta}(t)\cos(m\theta)+\sum_{m=1}^{\infty}C_{out,ms}^{\theta}(t)\sin(m\theta) \tag{12}$$

$$f_i(r,\theta)=\sum_{m=0}^{\infty}f_{imc}^{\theta}(r)\cos(m\theta)+\sum_{m=1}^{\infty}f_{ims}^{\theta}(r)\sin(m\theta) \tag{13}$$

Making use of the orthogonality condition in the azimuthal direction inherent for the generalized Fourier series expansion for the volumetric heat source term yields

$$g_{i0}^{\theta}(r,t)=\frac{1}{N_{\theta m}}\int_0^{2\pi}g_i(r,\theta,t)d\theta,\ \text{for } m=0 \tag{14}$$

$$g_{imc}^{\theta}(r,t)=\frac{1}{N_{\theta m}}\int_0^{2\pi}g_i(r,\theta,t)\cos(m\theta)d\theta,\ \text{for } m\neq 0 \tag{15}$$

$$g_{ims}^{\theta}(r,t)=\frac{1}{N_{\theta m}}\int_0^{2\pi}g_i(r,\theta,t)\sin(m\theta)d\theta,\ \text{for } m\neq 0 \tag{16}$$

with

$$N_{\theta m}=\begin{cases}\pi, \text{ when } m\neq 0\\ 2\pi, \text{ when } m=0\end{cases} \tag{17}$$

where the exact same expressions provided in Eqs. (*14*)-(*16*) , as well as the normalization factor $N_{\theta m}$ in Eq. (17), are valid to reduce $C_{in}(\theta,t)$ to $C_{in,m}^{\theta}(t)$, $C_{out}(\theta,t)$ to $C_{out,m}^{\theta}(t)$ and $f_i(r,\theta)$ to $f_{im}^{\theta}(r)$.

Reducing the 2-D heat conduction PDE by the application of the Fourier Series expansion yields m 1-D PDEs sets formed considering each positive integer value of m, written as

$$\frac{1}{\alpha_i}\frac{\partial T_{im}^{\theta}}{\partial t}(r,t)=\frac{1}{r}\frac{\partial}{\partial r}\left(r\frac{\partial T_{im}^{\theta}}{\partial r}(r,t)\right)-\frac{m^2}{r^2}T_{im}^{\theta}(r,t)+\frac{g_{im}^{\theta}(r,t)}{k_i} \tag{18}$$

where for now on the c and s subscripts will be omitted for sake of brevity. These subscripts will be recalled in the final solution to remind the reader that, throughout the mathematical modeling, the subscripts were suppressed.

The final reduced boundary and initial conditions are expressed as follows

$$A_{in}\frac{\partial T_{1m}^{\theta}}{\partial r}(r_0,t)+B_{in}T_{1m}^{\theta}(r_0,t)=C_{in,m}^{\theta}(t) \tag{19}$$

$$A_{out}\frac{\partial T_{nm}^{\theta}}{\partial r}(r_n,t)+B_{out}T_{nm}^{\theta}(r_n,t)=C_{out,m}^{\theta}(t) \tag{20}$$

$$T_{im}^{\theta}(r,t=0)=f_{im}^{\theta}(r) \tag{21}$$

and the reduced interfacial conditions are written as follows

$$T_{im}^{\theta}(r_{i-1},t)=T_{i-1,m}^{\theta}(r_{i-1},t) \tag{22}$$

$$k_i\frac{\partial T_{im}^{\theta}}{\partial r}(r_{i-1},t)=k_{i-1}\frac{\partial T_{i-1,m}^{\theta}}{\partial r}(r_{i-1},t) \tag{23}$$

2.2 Modifying the 1-D reduced governing equations

The reduced temperature field can be obtained by splitting the modified governing equation given in Eq. (18) into a transient homogeneous term and the inhomogeneous pseudo steady state problem, cast as

$$T_{im}^{\theta}(r,t)=\overline{T}_{im}^{\theta}(r,t)+T_{ss,im}^{\theta}(r,t) \tag{24}$$

where the homogeneous transient problem is expressed as

$$\frac{1}{\alpha_i}\frac{\partial\overline{T}_{im}^{\theta}}{\partial t}(r,t)=\frac{1}{r}\frac{\partial}{\partial r}\left(r\frac{\partial\overline{T}_{im}^{\theta}}{\partial r}(r,t)\right)-\frac{m^2}{r^2}\overline{T}_{im}^{\theta}(r,t)+\frac{\overline{g}_{im}^{\theta}(r,t)}{k_i},\ r_{i-1}\le r\le r_i,\ 1\le i\le n \tag{25}$$

and the reduced modified volumetric heat source, $\overline{g}_{im}^{\theta}(r,t)$, is cast as

$$\overline{g}_{im}^{\theta}(r,t)=k_i\left[\frac{1}{r}\frac{\partial}{\partial r}\left(r\frac{\partial T_{ss,im}^{\theta}}{\partial r}(r,t)\right)-\frac{m^2}{r^2}T_{ss,im}^{\theta}(r,t)-\frac{1}{\alpha_i}\frac{\partial T_{ss,im}^{\theta}}{\partial t}(r,t)\right]+g_{im}^{\theta}(r,t) \tag{26}$$

Due to the pseudo steady state condition, the first two terms within the brackets on the RHS of Eq. (26) are neglected, yielding

$$\overline{g}_{im}^{\theta}(r,t)=-\frac{k_i}{\alpha_i}\frac{\partial T_{ss,im}^{\theta}}{\partial t}(r,t)+g_{im}^{\theta}(r,t),\ r_{i-1}\le r\le r_i,\ 1\le i\le n \tag{27}$$

The reduced modified inner and outer boundary conditions and initial condition are

$$A_{in}\frac{\partial\overline{T}_{im}^{\theta}}{\partial r}(r_0,t)+B_{in}\overline{T}_{im}^{\theta}(r_0,t)=0 \tag{28}$$

$$A_{out}\frac{\partial\overline{T}_{im}^{\theta}}{\partial r}(r_n,t)+B_{out}\overline{T}_{im}^{\theta}(r_n,t)=0 \tag{29}$$

$$\overline{f}_{im}^{\theta}(r)=f_{im}^{\theta}(r)-T_{ss,im}^{\theta}(r,t=0) \tag{30}$$

and the reduced modified interfacial conditions at the $(i-1)$st and at the ith layer, for $i=2,\ldots,n$ are written as

$$\overline{T}_{im}^{\theta}(r_{i-1},t)=\overline{T}_{i-1,m}^{\theta}(r_{i-1},t) \tag{31}$$

$$k_i\frac{\partial\overline{T}_{im}^{\theta}}{\partial r}(r_{i-1},t)=k_{i-1}\frac{\partial\overline{T}_{i-1,m}^{\theta}}{\partial r}(r_{i-1},t) \tag{32}$$

2.3 Temperature Fields Solution

The solution of the inhomogeneous pseudo steady state problem exists if it can be written as linear combination of functions that involves, separately, the product between a spatial-dependent and a temporal-dependent components, characterizing a separable function. Thus, this linear combination, for each layer, yields

$$T_{ss,im}^{\theta}(r,t)=T_{im}^{\theta,\psi}(r)C_{in,m}^{\theta}(t)+T_{im}^{\theta,\phi}(r)C_{out,m}^{\theta}(t) \tag{33}$$

where $T_{im}^{\theta,\psi}(r)$ and $T_{im}^{\theta,\phi}(r)$ are determined as follows

$$T_{im}^{\theta}(r) = A_{ss,i}u_m(r) + B_{ss,i}v_m(r) \tag{34}$$

with the r dependent terms calculated as

$$u_m(r) = \begin{cases} \ln r, \text{ if } m = 0 \\ r^m, \text{ if } m \neq 0 \end{cases}, \text{ and } v_m(r) = r^{-m} \tag{35}$$

The application of the inner, outer and interfacial boundary conditions enables one to determine the coefficients $A_{ss,i}$ and $B_{ss,i}$ available in Eq. (34), resulting in a coefficient matrix representation of size $(2n \times 2n)$ and a vector of size $(2n \times 1)$ containing the boundary excitations.

The solution of the homogeneous transient problem is obtained applying the FIT technique operating the pair $k_i \int_{r_{i-1}}^{r_i} rR_{im}(r)dr$ in the homogeneous governing equation. The solution yields

$$T_{mp}^{r\theta}(t) = \left[T_{mp}^{r\theta}(t=0) + \int_0^t \left(T_{ss,mp}^{r\theta}(\tau) + g_{im}^{r\theta}(\tau) \right) e^{\alpha_1 \lambda_{1mp}^2 \tau} d\tau \right] e^{-\alpha_1 \lambda_{1mp}^2 t} \tag{36}$$

with

$$T_{mp}^{r\theta}(t) = \sum_{i=1}^{n} \frac{k_i}{\alpha_i} \int_{r_{i-1}}^{r_i} rR_{imp}(r) \bar{T}_{im}^{\theta}(r,t) dr \tag{37}$$

$$g_{mp}^{r\theta}(t) = \sum_{i=1}^{n} -\frac{k_i}{\alpha_i} \int_{r_{i-1}}^{r_i} rR_{imp}(r) \left[\frac{\partial T_{ss,im}^{\theta}}{\partial t}(r,t) \right] dr + \sum_{i=1}^{n} \int_{r_{i-1}}^{r_i} rR_{imp}(r) g_{im}^{\theta}(r,t) dr \tag{38}$$

$$T_{mp}^{r\theta}(0) = \sum_{i=1}^{n} \frac{k_i}{\alpha_i} \int_{r_{i-1}}^{r_i} rR_{imp}(r) \left(f_{im}^{\theta}(r) - T_{ss,im}^{\theta}(r, t=0) \right) dr \tag{39}$$

The application of the generalized Fourier series expansion in the reduced-modified homogeneous transient temperature problem yields

$$\bar{T}_{im}^{\theta}(r,t) = \sum_{p=1}^{\infty} c_{mp}(t) R_{imp}(r) \tag{40}$$

where $c_{mp}(t)$ is the time-dependent coefficient. The orthogonality condition that arises on the series expansion in Eq. (40) is written as

$$c_{mp}(t) = \frac{T_{mp}^{r\theta}(t)}{N_{mp}} \tag{41}$$

where the normalization factor in the radial direction is determined as follows

$$\sum_{i=1}^{n} \frac{k_i}{\alpha_i} \int_{r_{i-1}}^{r_i} rR_{imp}(\lambda_{imp} r) R_{imq}(\lambda_{imq} r) dr = \begin{cases} 0 & \text{if } p \neq q \\ N_{mp} & \text{if } p = q \end{cases} \tag{42}$$

The eigenfunction problem of the homogeneous transient governing equation is given as

$$R_{imp}\left(\lambda_{imp}r\right)=a_{imp}J_m\left(\lambda_{imp}r\right)+b_{imp}Y_m\left(\lambda_{imp}r\right) \tag{43}$$

with J_m and Y_m being *m*-order Bessel functions of the first and second kinds, respectively, and a_{imp} and b_{imp} the associated Bessel function coefficients. The p subscript is associated to the eigenvalue problem in the *r*-direction. For each reduced-modified m sets of 1-D PDEs exists an infinite number of eigenvalues, λ_{imp}, for each *i*th layer $\lambda_{1mp}<\lambda_{2mp}<\lambda_{3mp}<...<\lambda_{nmp}<...$ (Özisik, 1993).

Substituting both homogeneous boundary and interfacial conditions, the eigenvalues associated to the eigenfunction problem of each of the *i*th-layer of the composite hollow cylinder domain results in a coefficient matrix representation of size $\left(2n\times 2n\right)$ multiplied by a $\left(2n\times 1\right)$ vector that carries the Bessel function coefficients a_{imp} and b_{imp}. Operating the determinant of the coefficient matrix equal to zero, the roots of the resulting expression return the solution of the eigenvalue problem in the radial direction. Then the Bessel functions coefficients a_{imp} and b_{imp} are prompt to be determined.

After both reduced-modified inhomogeneous pseudo steady state, $T^{\theta}_{ss,im}\left(r,t\right)$, and the homogenous transient temperature problems in Eqs. (33) and (40), respectively, it is possible to recover the reduced form of the temperature, $T^{\theta}_{im}\left(r,t\right)$, by means of Eq. (24).

Lastly the transient reduced governing equation is applied in Eq. (9), recovering the original transient heat conduction problem cast in 2-D radial-azimuthal coordinates, $T_i\left(r,\theta,t\right)$. This task may be accomplished after summing over m=1 to m=M sets of reduced 1-D PDEs, where for each integer value of m considered herein exists a set of p radial eigenvalues associated.

Thus, rewriting Eq. (9) in view of both the reduced-modified homogeneous transient and the pseudo steady state heat conduction problems, and recalling the *c* and *s* subscripts associated to the oscillatory functions that arises from the generalized Fourier series expansion, the final solution may be obtained as

$$\begin{aligned}T_i\left(r,\theta,t\right)=&\sum_{m=1}^{\infty}\left(\sum_{p=1}^{\infty}\frac{T^{r\theta}_{mpc}\left(t\right)}{N_{mp}}R_{imp}\left(r\right)+T^{\theta}_{ss,im}\left(r,t\right)\right)\cos\left(m\theta\right)+\\ &\sum_{m=1}^{\infty}\left(\sum_{p=1}^{\infty}\frac{T^{r\theta}_{mps}\left(t\right)}{N_{mp}}R_{imp}\left(r\right)+T^{\theta}_{ss,im}\left(r,t\right)\right)\sin\left(m\theta\right)+\left(\sum_{p=1}^{\infty}\frac{T^{r\theta}_{0p}\left(t\right)}{N_{0p}}R_{i0p}\left(r\right)+T^{\theta}_{ss,i0}\left(r,t\right)\right)\end{aligned} \tag{44}$$

3. RESULTS AND DISCUSSION

The analytical and numerical investigations were conducted on the two-dimensional multilayered physical domain illustrated in Figure 2. The domain is composed of a solid circular area that may be obtained by slicing the cross section of the well structure. The heat transfer between the resultant area and the materials right above or below it is assumed to be zero.

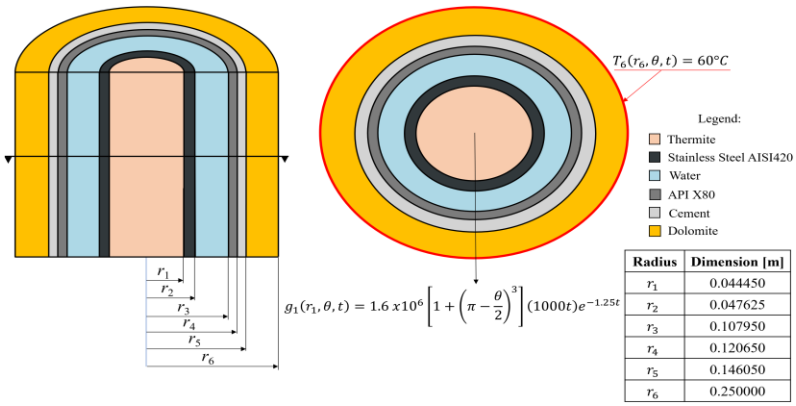

Radius	Dimension [m]
r_1	0.044450
r_2	0.047625
r_3	0.107950
r_4	0.120650
r_5	0.146050
r_6	0.250000

Figure 2 – Six-layers solid cylinder representing the oil well assembly (left) and two-dimensional physical domain (right).

Here, the g_1 (r, θ, t) is a temporal-spatial dependent heat source function set in the innermost layer (thermite). The outermost boundary (in dolomite subdomain) was set as a fixed temperature equal to its initial value. For offshore oil wells, an average initial temperature value of 60.0 °C is verified (Abdelal, Robotham, & Carragher, 2015).

The geometrical, thermophysical and physical properties of an average offshore oil well structure are cast in Table 1 and were retrieved from the open literature (Durães, Brito, Campos, & Portugal, 2006), (Zhang, Farahmand, & Kovacevic, 2016), (Chunyan, Cuiying, & Bo, 2014), (Xu & Chung, 2000), (Eppelbaum, Kutasov, & Pilchin, 2014), (Rocha, et al., 2018), 1440 (Da Nóbrega, et al., 2016), (Bouhifd, et al., 2006) .

Table 1. Geometrical, thermophysical, and physical properties of an average offshore oil well structure (as in Figure 2).

Material	Thermite	SS AISI 420	Water	API X80	Cement	Dolomite
Radius (r) [m]	0.044450	0.047625	0.107950	0.120650	0.146050	0.250000
Density (ρ) [kg/m³]	4142	7671	998	7800	2010	953
Thermal Conductivity (k) [W/m.K]	47.88	26.08	0.65	54.21	0.53	3.34
Specific Heat (c_p) [J/kg.K]	748.10	475.61	4185	448	736	2630

Analyzing the temperature evolution measured at times $t = 50s$, $t = 150s$, $t = 300s$, $t = 500s$ and $t = 1000s$ $t = 1000\text{s}$, the resultant transient behavior through the radial direction for the fixed azimuthal angle values of $\theta = 30°$ and $\theta = 225°$ are plotted in Figure 3. The graphs show the asymmetrical behavior due to the proposed spatial-temporal dependent heat source profile.

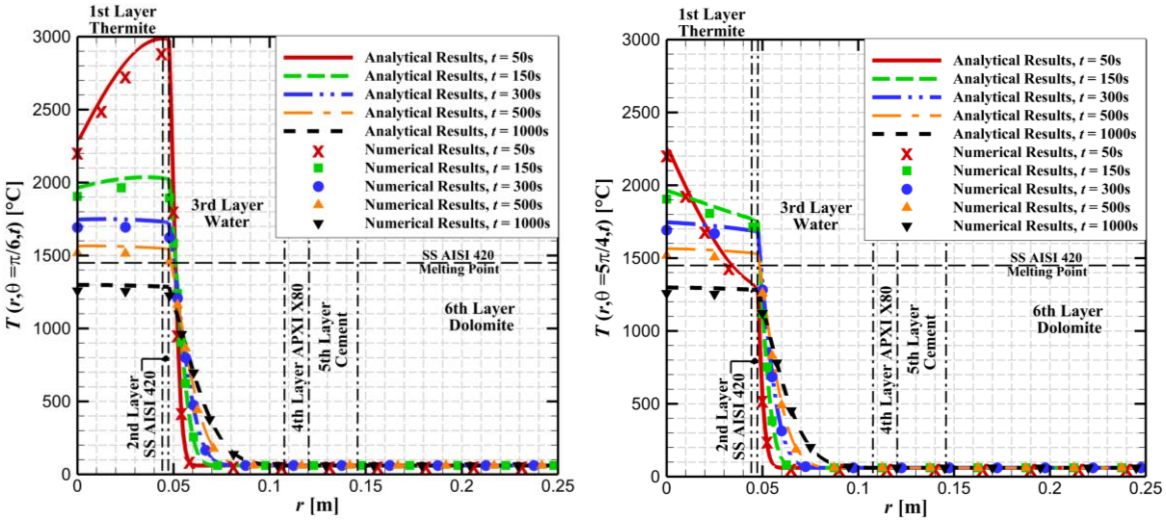

Figure 3 – Transient temperature profiles (T [°C]) along the radial coordinate (r [m]), for the times $t = 50s$, $t = 150s$, $t = 300s$, $t = 500s$ and $t = 1000s$, and settling the azimuthal direction at: a) $\theta = \pi / 6$, b) $\theta = 3\pi / 4$, c) $\theta = 5\pi / 4$, d) $\theta = 7\pi / 4$.

The vertical dashed lines in Figure 3 indicates the layer interfaces positions at $r_1 = 0.04445m$, $r_2 = 0.047625m$, $r_3 = 0.10795m$, $r_4 = 0.12065m$ and $r_5 = 0.14605m$. The horizontal dashed line at the temperature of 1450°C indicates the melting point threshold of the SS AISI 420 for the layer thickness comprehended within the range $r_1 \le r \le r_2$. At this layer relies the main engineering interest in the investigation, since the first requirement of the intermediate milestone of the TP&A proposal is to achieve the complete melting of the production tube.

In view of Figure 3a, the temperature fields remain above the melting temperature for all considered times (except for $t = 1000s$). In Figure 3b on the other hand, when $t = 50s$ the temperature field diminishes faster than in comparison with $\theta = \pi / 6$, where the turning-point occurs at $r = 0.03422$ m , resulting in $r < r_1$. Such occurrence indicates that even at its innermost surface, the production tube does not experience sufficient temperature levels to start the melting phenomena. At r_1 and $t = 50s$ for $\theta = 5\pi / 4$, the measured temperature provided by the analytical approach equals to 1328 °C.

From the evaluation of Figure 3b arises the necessity to thoroughly analyze the azimuthal direction instead of just fixing it, since some angular portion at specific times could not surpass the melting temperature threshold, as observed at $t = 50s$ for $\theta = 5\pi / 4$. The main contribution of an azimuthal evaluation relies on the fact that the second intermediate milestone may be better investigated, which requirements demands that the cement pumped downhole meets the gap formed by the molten section. Here, it is assumed that the fused SS AISI420 portion moves down, is deposited, and solidified right below the destroyed section. Hence, the solidification product is not only assumed to not obstruct the gap and but also to become an integrating part of the plug consolidation. The resultant space finally allows enough room for the cement flow, thus occupying the oil well cross section. The transient temperate profiles for each of the previous defined time-step values, varying from $0 < \theta < 2\pi$ and measured at the $(i-1)$th layer interfaces for $i = 1, 2, 3, \ldots, 6$ are plotted in Fig. 4.

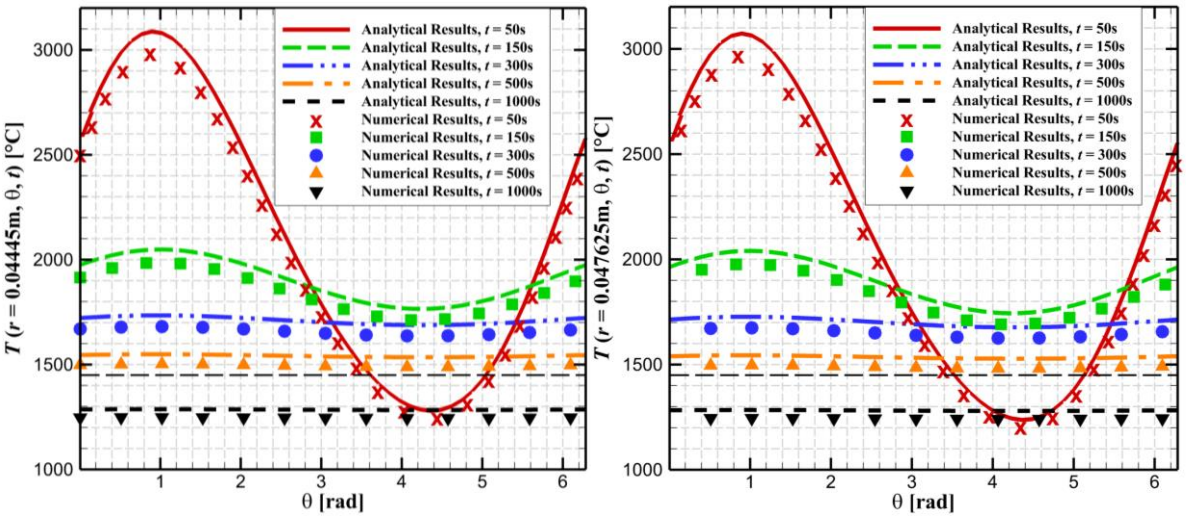

a) b)

Figure 4 – Transient temperature fields (T [°C]) along the azimuthal coordinate, for the times t = 50 s, t = 150 s, t = 300 s, t = 500 s, t = 1000 s, and settling the radial coordinate at: a) $r_1 = 0.04445m$, b) $r_2 = 0.047625m$.

Analyzing Figure 4a and Figure 4b, the phenomena where a portion of the circumference is melted only occurs for $t = 50s$ while the measurements at the other time values does not experience phase change. The angular intervals where the azimuthal coordinate remains above the melting temperature of the SS AISI 420 for both numerical and analytical approaches are tabulated in Table 2. As the second intermediate milestone requirement demands that the whole production tube thickness must be melted, the results that will be considered herein are those settled at the $r_2 = 0.047625m$ interface. A total of 267.99° of the azimuthal portions remains above the melting temperature

Table 2. Azimuthal portions where the temperature threshold remains above the melting point in view of Figure 4.

	Thermite / SS AISI 420 Interface (Figure 4a)		SS AISI 420 / Water Interface (Figure 4b)	
Time	θ[rad]	θ[°]	θ[rad]	θ[°]
Analytical $t = 50s$	0 - 3.613 5.039 - 6.283	0 - 206.996 288.705 – 360.000	0 - 3.525 5.131 - 6.283	0 - 201.973 293.978 – 360.000
Melted angle [°]	4.857	278.29°	4.677	267.99°

The contour plots of the resultant temperature distribution are available in Figure 5. The images were extracted for the fixed time-step values of $t = 50$ s, $t = 150$ s, $t = 300$ s, $t = 500$ s, $t = 1000$ s and shows the asymmetrical nature of the space-temporal dependent heat source profile discretized as the heat source arising from the thermite reaction. The temperature fields tend to stabilize with the time evolution, where for $t = 50$ s the melted portion is evident. It is roughly perceptive that almost three quarters of the SS AISI 420 effectively achieves its melting temperature for its whole thickness ($r_2 = 0.047625$ m). Adding to the previous discussion, it is also possible to notice that starting from the water layer, the temperature levels greatly decay to the initial condition of 60°C, thus guaranteeing that any harmful effects caused to high temperatures in the cement layer are mitigated.

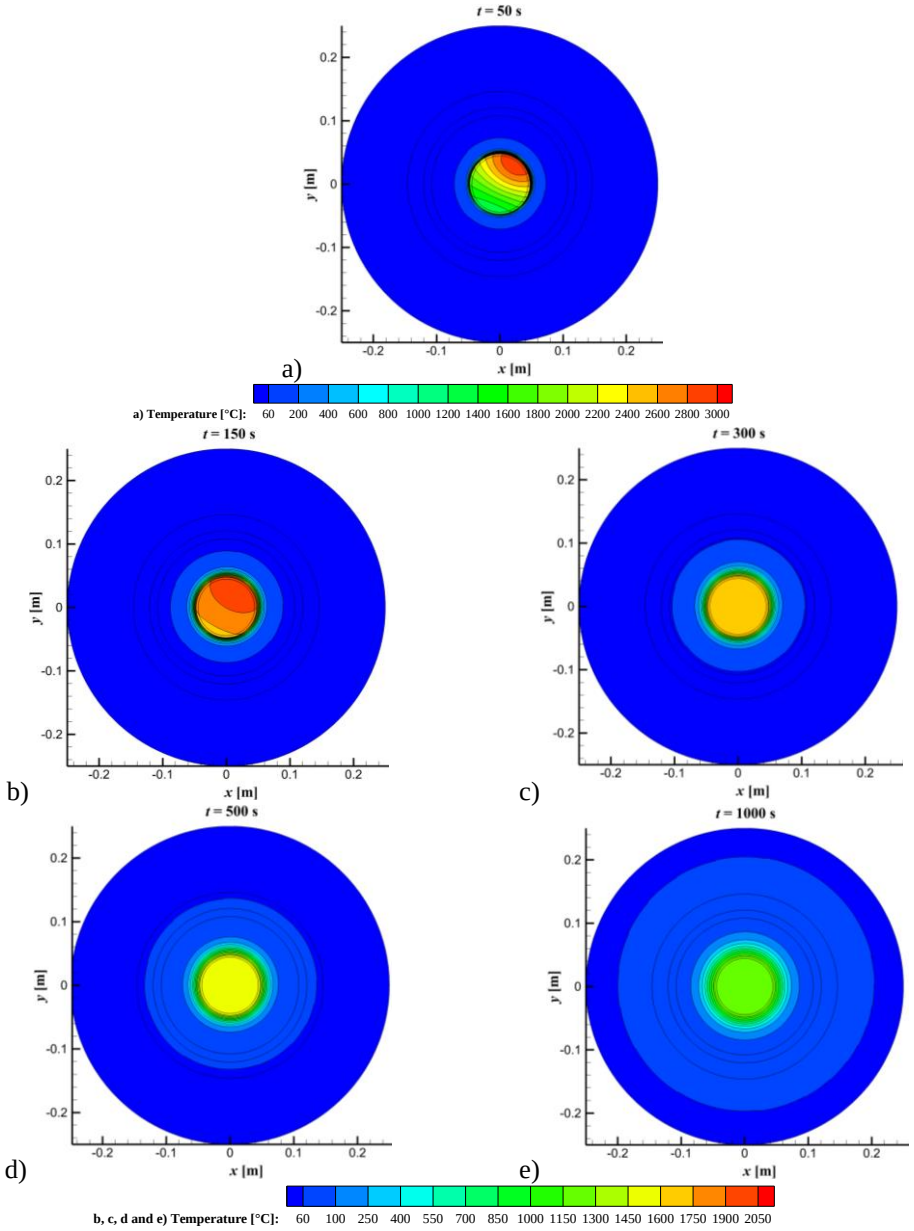

Figure 5 – Temperature contours (T) [ºC] as a function of cartesian coordinates (x, y) [m] and time (t) [s] for: a) t = 50 s, b) t = 150 s, c) t = 300 s, d) t = 500 s, e) t = 1000 s.

4. CONCLUSION

An investigation of the TP&A technique for permanently sealing oil wells was conducted in the present study. Here, an intermediate milestone involving the hybrid use of a thermite heat emitter device and the traditional cementing technique was investigated. The first requirement established that the resultant temperatures at the production column should be high enough to achieve fusion. The second step consisted in ensuring that even in the event of a partial reaction failure or a highly uneven heat transfer pattern to the production tube, at least a small angular section of it would be fused. Hence, the FIT analytical framework was applied to calculate the resultant temperature fields due to its capability of handling time-dependent boundary conditions and a spatial-temporal dependent heat source term. The FVM was also applied to produce an equivalent solution and allow the comparison of both outcomes, thus increasing the reliability of the study.

The yielded temperatures gave insight that during the 1000 s analyzed, any point contained in the area delineated by $r \leq 0.047625$ m was indeed submitted to temperatures above the melting point of the SS AISI 420 steel, thus fulfilling the first step of the milestone requirements. However, as the melting process absorbs energy through the latent heat of fusion, it is not possible to assure that the entire azimuthal length of the tube would experience complete liquefication. It was estimated from the results that the heat levels achieved are capable of melting at least nearly three-quarters ($\theta_m = 3\pi/2$) of the production tube's azimuthal length.

5. REFERENCES

Aas, B., Sørbø, J., Stokka, S., Saasen, A., Statoil, R. G., Lunde, Ø., Phillips, C. and Vrålstad, T., 2016. Cement Placement with Tubing Left in Hole during Plug and Abandonment Operations. Drilling Conference and Exhibition. Fort Worth, Texas, USA: IADC/SPE.

Abdelal, G. F., Robotham, A. and Carragher, P., 2015. Numerical simulation of a patent technology for sealing of deep-sea oil wells using nonlinear finite element method. Journal of Petroleum Science and Engineering, pp.192-200.

Abshire, L. W., Desai, P., Mueller, D., Paulsen, W. B., Robertson, R. D. and Solheim, T., 2012. Offshore permanent well abandonment. Oilfield Review, Vol. 24, no. 1, pp. 42 - 50.

Biswas, P., Singh, S. and Bindra, H., 2019. Homogenization of Time Dependent Boundary Conditions for Multi-layer Heat Conduction Problem in Cylindrical Polar Coordinates. International Journal of Heat and Mass Transfer, Vol. 129, pp.721-734.

Bouhifd, M. A., Besson, P., Courtial, P., Gérardin, C., Navrotsky, A. and Richet, P., 2006. Thermochemistry and melting properties of basalt. Contributions to Mineralogy and Petrology, Vol. 153, pp. 689-698.

Chunyan, Y., Cuiying, L. and Bo, Y., 2014. 3D modeling of the hydrogen distribution in X80 pipeline steel welded joints. Computational Materials Science, Vol. 83, pp. 158-163.

Da Nóbrega, J. A., Diniz, D. D., Silva, A. A., Maciel, T. M., De Albuquerque, V. H. and Tavares, J. R., 2016. Numerical Evaluation of Temperature Field and Residual Stresses in an API 5L X80 Steel Welded Joint Using the Finite Element Method. Metals, Vol. 6, no. 2.

de Andrade, G. S., de Lemos, M. J. and Colombo, D., 2021. A new hybrid analytical/numerical method for transient heat conduction on composite hollow cylinders applied to plug and abandonment of oil wells. International Journal of Thermal Sciences, Vol. 168.

de Andrade, G. S., Nascimento, E. J. and de Lemos, M. J., 2023. Analytical solution of two-dimensional unsteady heat conduction in multi-layered cylindrical sectors applied to thermal plug and abandonment of oil wells. International Journal of Thermal Sciences, pp. 108180.

Durães, L., Brito, P., Campos, J. and Portugal, A., 2006. Modelling and simulation of Fe2O3/Aluminum thermite combustion: Experimental validation. Computer Aided Chemical Engineering, Vol. 21, pp. 365-370.

Eppelbaum, L., Kutasov, I. and Pilchin, A., 2014. Chapter 2 - Thermal Properties of Rocks and Density of Fluids. In Applied Geothermics, pp. 99-149. New York: Springer.

Gu, Y. and O'Neal, D. L., 1995. An Analytical Solution to Transient Heat Conduction in a Composite Region With a Cylindrical Heat Source. Journal of Solar Energy Engineering, Vol. 117, no. 3, pp. 242 - 248.

Moeinikia, F., Fjelde, K. K., Sørbø, J., Saasen, A. and Vrålstad, T., 2015. A Study of Possible Solutions for Cost Efficient Subsea Well Abandonment. 34th International Conference on Ocean, Offshore and Arctic Engineering (pp. OMAE2015-41261). St. John's, Newfoundland, Canada: ASME.

Ouyang, S. and Allen, E., 2017. Offshore well abandonment: challenges and approach with DNV GL guideline of risk-based abandonment. Journal of Offshore Engineering Technology, Vol. 1, no. 1, pp. 71 - 83.

Özisik, M. K., 1993. Heat Conduction: 2nd Edition. New York: John Wiley & Sons.

Rocha, E. J., Antonino, T. d., Guimarães, P. B., Ferreira, R. A., Barbosa, J. M. and Rohatgi, J., 2018. Modeling of the temperature field generated by the deposition of weld bead on a steel butt joint by FEM techniques and thermographic images. Materials Research, Vol. 21, no. 3.

Torabi, M. and Zhang, K., 2016. Analytical Solution for Transient Temperature and Thermal Stresses within Convective Multilayer Disks with Time-Dependent Internal Heat Generation, Part I: Methodology. Journal of Thermal Stresses, Vol. 39, pp. 398-413.

Vrålstad, T., Saasen, A., Fjær, E., Øia, T. and Ytre, J. D., 2019. Plug & abandonment of offshore wells: ensuring long-term well integrity and cost efficiency, Journal of Petroleum Science and Engineering, pp. 478-491.

Wang, H., Duan, M., An, C. and Su, J., 2021. Lumped parameter thermal analysis of multilayered composite pipe with MicroPCM particles. Composite Structures.

Xu, Y. and Chung, D. D., 2000. Effect of sand addition on the specific heat and thermal conductivity of cement. Cement and Concrete Research, Vol. 30, pp. 59-61.

Zhang, G., Xia, C., Sun, M., Zou, Y. and Xiao, S., 2013. A new model and analytical solution for the heat conduction of tunnel lining ground heat exchangers. Cold Regions Science and Technology, Vol. 88, pp. 55-66.

Zhang, Z., Farahmand, P. and Kovacevic, R., 2016. Laser cladding of 420 stainless steel with molybdenum on mild steel A36 by a high power direct diode laser. Materials & Design, Vol. 109, pp. 686 - 699.

6. RESPONSIBILITY NOTICE

The authors are the only responsible for the printed material included in this paper.